ELSEVIER

Surface Science 414 (1998) 159–169

surface science

Surface atomic structure of the $(\sqrt{3} \times \sqrt{3})R30^{\circ}$-Sb reconstructions of Ag(111) and Cu(111)

S.A. de Vries [a,*], W.J. Huisman [a], P. Goedtkindt [a,b], M.J. Zwanenburg [a,1], S.L. Bennett [c], I.K. Robinson [d], E. Vlieg [a,e]

[a] *FOM Institute for Atomic and Molecular Physics, Kruislaan 407, 1098 SJ Amsterdam, The Netherlands*
[b] *Department of Chemistry, Universitaire Instelling Antwerpen, Universiteitsplein 1, B-2610 Wilrijk, Belgium*
[c] *CCLRC, Daresbury Laboratory, Warrington, WA4 4AD, UK*
[d] *University of Illinois, Urbana, IL 61801, USA*
[e] *RIM, Department of Solid State Chemistry, University of Nijmegen, Toernooiveld 1, 6525 ED Nijmegen, The Netherlands*

Received 30 April 1998; accepted for publication 15 June 1998

Abstract

We present an X-ray diffraction structure analysis of the $(\sqrt{3} \times \sqrt{3})R30^{\circ}$ reconstructions of Ag(111)-Sb and Cu(111)-Sb surfaces. We find these structures to be very similar. Contrary to previous reports, we find that all top layer atoms reside at stacking fault positions. Each $(\sqrt{3} \times \sqrt{3})R30^{\circ}$ surface unit cell contains one substitutional Sb atom. We determined the out-of-plane relaxations of the top layer atoms and the in-plane distortions in the second layer. For coverages below 1/3 monolayer, the Sb atoms are embedded randomly at fcc positions in the top surface layer.

Keywords: Antimony; Copper; Low-index single-crystal surfaces; Silver; Surface structure; X-ray scattering, diffraction, and reflection

1. Introduction

Interest in homoepitaxial metal growth has increased enormously in recent years. Egelhoff and Jacob [1] showed that metal layers can grow layer-by-layer at unexpectedly low temperatures. Another interesting observation was made by Kunkel et al. [2], who discovered re-entrant layer-by-layer growth at low temperatures in the growth of Pt on Pt(111). Van der Vegt et al. [3] were the first to show that surfactants can be used to induce layer-by-layer metal growth.

In homoepitaxy, simple kinetic processes influencing epitaxial growth can be studied without complicating effects such as lattice mismatch or differences in surface energy. It has been known for some time that epitaxial growth of metals can be influenced by a variety of adsorbed gases [4–7], but only recently has it been shown that for a number of metals smooth homoepitaxial growth can be stimulated by using surfactants like Sb, O_2 and In [3,8–10]. Understanding the origin of the various phenomena occurring in homoepitaxy is important for deriving conclusions applicable to

* Corresponding author. Fax: +31 20 6684106; e-mail: devries@amolf.nl

[1] Present address: University of Amsterdam, Van der Waals–Zeeman Institute, Valckenierstraat 65, 1018 XE Amsterdam, The Netherlands.

0039-6028/98/$ – see front matter
PII: S0039-6028(98)00509-3

the more complex heteroepitaxial systems, like metallic multilayers, which are interesting as magnetic materials.

Sb is widely used as a surfactant because of its low surface energy. Submonolayer coverages of Sb change the growth mode of Ag(111) from multilayer (3D) growth to layer-by-layer (2D) growth [3]. Very recently we have found that during Ag growth, predeposition of Sb may lead to a top layer with the wrong stacking [11]. The surfactant effect of Sb is closely related to its strong tendency to segregate, but despite the increased interest in the use of surfactants in metal growth, the microscopic mechanisms of dissolution and segregation of Sb are at present not fully understood [12]. The surfactant effect is dependent on the coverage, and the occurrence of a $(\sqrt{3}\times\sqrt{3})R30^\circ$ reconstruction may also play a role [13,14]. A prerequisite for better understanding of these phenomena is knowing the surface atomic structure. There has been, however, relatively little published on the structure of submonolayer coverages of Sb on clean metal surfaces.

For Ag(111), ab initio calculations [15] predict that for coverages up to 1/3 monolayer (ML) Sb is embedded in the top surface layer at substitutional sites. A $(\sqrt{3}\times\sqrt{3})R30^\circ$ reconstruction is formed at 1/3 ML. These predictions are confirmed by experimental studies [12,16–18]. At approximately double the Sb coverage a $(2\sqrt{3}\times2\sqrt{3})R30^\circ$ reconstruction is reported for annealing temperatures between 100 and 200°C [17]. No exact atomic coordinates have been derived from these studies.

Dissolution in the bulk of Sb after deposition of 1 ML on Cu(111) at 400°C takes place to leave a surface concentration of 1/3 ML with a $(\sqrt{3}\times\sqrt{3})R30^\circ$ reconstruction [19,20]. The segregation kinetics at the same temperature of Sb to the surface of a Cu(Sb)(111) solid solution (0.45 at%) similarly give rise to this $(\sqrt{3}\times\sqrt{3})R30^\circ$ reconstruction at the same surface Sb concentration. The dissolution and segregation kinetics are thus closely linked to the equilibrium surface segregation. Since the $(\sqrt{3}\times\sqrt{3})R30^\circ$ reconstruction can be formed by either segregation or dissolution, we conclude that this must be an equilibrium structure.

On Au(111), also a noble metal, no $(\sqrt{3}\times\sqrt{3})R30^\circ$ reconstruction is observed, but rather a $(2\sqrt{3}\times2\sqrt{3})R30^\circ$ structure forms, which is proposed to be a surface alloy of $AuSb_2$ stoichiometry, where the Sb atoms again occupy substitutional sites [21].

In this paper, we present an X-ray diffraction structure determination of the Ag(111) $(\sqrt{3}\times\sqrt{3})R30^\circ-Sb$ and Cu(111)$(\sqrt{3}\times\sqrt{3})R30^\circ-Sb$ surfaces. Surface X-ray diffraction has proved to be an excellent technique for determining atomic positions with a high degree of accuracy [22]. Our analysis is based upon comparison of calculated model structure factors with the distribution of diffracted intensities along rods of scattering perpendicular to the surface. These so-called crystal truncation rods (CTRs) originate from the abrupt truncation of the crystal lattice at the surface [23,24] and are diffuse tails whose intensity is given by the interference between bulk and surface atomic structure. We also measured fractional order reflections which are caused by the reconstruction and yield information about the atomic arrangement in the surface unit cell only. For both reconstructions, we find a similar atomic structure. A model featuring a top layer with one Sb atom and two Ag (or Cu) atoms in the surface unit cell at stacking fault positions describes our data best. This position has not been considered in the studies mentioned above.

2. Experimental

The measurements were performed at the surface X-ray diffraction station 9.4 of the 5 T wiggler beam line at the Synchrotron Radiation Source, Daresbury Laboratory, UK [25]. X-rays with a wavelength λ of 0.9 Å (13.8 keV) were selected using a channel-cut Si(111) monochromator. The set-up consists of an ultra-high vacuum chamber [26] coupled to a diffractometer. A Knudsen effusion cell was used for the Sb deposition at a rate of $\sim$0.002 ML/s. The deposition rate was estimated by assuming Poisson growth during deposition at low substrate temperatures. To prepare the surface reconstructions, Sb was deposited at

elevated temperatures, but both structure determinations were carried out at room temperature. The diffractometer, on which the sample was mounted with the surface normal lying in the horizontal plane, was operated in six-circle mode with the out-of-plane detector angle fixed at 0° or 15° [27,28].

We used round crystals with a diameter of 10 mm polished within $\sim 0.3^\circ$ of the crystallographic (111) plane. In order to remove the surface damage from the polishing treatment, both samples were first annealed to temperatures sufficient for significant sublimation to occur. The Ag(111) sample was annealed for 3.5 h at 700°C, reducing the surface mosaicity from 2° to 0.10° full-width at half-maximum (FWHM). After that, the sample was cleaned by repeated cycles of sputtering (600 eV Ar^+ at 300°C for 20 min) and annealing (600°C for 10 min). For Cu(111) an anneal treatment for 20 min at 900°C reduced the surface mosaicity from 1.1° to 0.08° FWHM. Thereafter the sample was cleaned by repeated cycles of sputtering at room temperature and annealing at 700°C.

The fcc crystals have an ABC stacking along the $\langle 111 \rangle$ direction. A hexagonal unit cell is employed to label the reflections (hkl). The lattice vectors $\{\boldsymbol{a}_i\}$ are expressed in terms of the conventional cubic lattice vectors by:

$$\boldsymbol{a}_1 = \tfrac{1}{2}[1\ 0\ \bar{1}]_{\text{cubic}},\ \boldsymbol{a}_2 = \tfrac{1}{2}[\bar{1}\ 1\ 0]_{\text{cubic}},$$
$$\boldsymbol{a}_3 = [1\ 1\ 1]_{\text{cubic}} \quad (1)$$

with

$$|\boldsymbol{a}_1| = |\boldsymbol{a}_2| = \tfrac{1}{2}\sqrt{2}a_0,\ |\boldsymbol{a}_3| = \sqrt{3}a_0$$

and a_0 the lattice constant of Ag (4.09 Å) or Cu (3.61 Å). The corresponding reciprocal lattice vectors $\{\boldsymbol{b}_i\}$ are defined by $\boldsymbol{a}_i \cdot \boldsymbol{b}_j = 2\pi\delta_{ij}$.

The momentum transfer vector $\boldsymbol{Q}$ is the difference between the outgoing wavevector $\boldsymbol{k}_{\text{out}}$ and the incoming wavevector $\boldsymbol{k}_{\text{in}}$ ($|\boldsymbol{k}_{\text{out}}| = |\boldsymbol{k}_{\text{in}}| = 2\pi/\lambda$) and is denoted by diffraction indices (hkl) in reciprocal space:

$$\boldsymbol{Q} = h\boldsymbol{b}_1 + k\boldsymbol{b}_2 + l\boldsymbol{b}_3 \quad (2)$$

Here the diffraction index pair (hk) refers to the in-plane component and the index l to the perpendicular component of $\boldsymbol{Q}$. For CTRs, which are labeled (hk), the indices h and k have integer values, whereas l is unconstrained. The perpendicular momentum transfer along the rods was varied by changing the incoming angle β_{in}, keeping the exit angle β_{out} fixed at 1°. In-plane data were collected using small incidence and exit angles ($\beta_{\text{in}} = \beta_{\text{out}} < 1^\circ$) corresponding to small values of perpendicular momentum transfer ($l = 0.2$). Slits in front of the Ge solid-state detector fixed the angular acceptance at 0.26° in the in-plane and 0.43° in the out-of-plane direction. These correspond to momentum resolutions of $\Delta Q = 0.03\ \text{Å}^{-1}$ and $0.05\ \text{Å}^{-1}$, respectively.

Integrated intensities at various values of l along a non-specular diffraction rod are determined by rotating the crystal about the surface normal and measuring the number of diffracted photons. The specular reflected intensity distribution along the $(h\,k) = (0\,0)$ rod is measured in a different way, namely using a "ridge" scan, in which the incident and exit angles are symmetrically incremented (keeping $\beta_{\text{in}} = \beta_{\text{out}}$). The intensity at different l values is measured by counting the scattered photons within the angular acceptance of the detector.

Structure factors are obtained by dividing the measured intensity by the Lorentz factor, the polarization factor, an area correction factor, and taking the square root. The Lorentz and polarization factors can be calculated analytically, the area correction is calculated numerically [29]. To do this we took for the beam profile a Gaussian line shape with a FWHM of 2 mm in the horizontal and 0.6 mm in the vertical direction.

We start our analysis with model structure factors calculated for a given atomic arrangement in the unit cell. To calculate the contribution arising from the bulk of the crystal, F_{hkl}^{bulk}, we describe the crystal by slicing it in columns perpendicular to the surface having a (1×1) periodicity. Subsequently, we section the columns into (111) layers and sum over all the layers. Each layer contains only one atom and the structure factor for a single layer is just

$$F_{hkl}^{\text{layer}} = f^{hkl} \exp\left(\frac{-B\boldsymbol{Q}^2}{16\pi^2}\right) \quad (3)$$

where f^{hkl} is the atomic form factor and B is the isotropic Debye–Waller parameter. Throughout we assume the value of B to be equal to the room temperature bulk value of 0.66 Å^2 for Ag and 0.55 Å^2 for Cu [30]. Each layer is shifted over a translation vector $\boldsymbol{r}^{\text{layer}} = \frac{2}{3}\boldsymbol{a}_1 + \frac{1}{3}\boldsymbol{a}_2 + \frac{1}{3}\boldsymbol{a}_3$. For the nth layer this results in a phase shift $\exp(in\psi_{hkl})$ with:

$$\psi_{hkl} = \boldsymbol{Q}\cdot\boldsymbol{r}^{\text{layer}} = 2\pi(\tfrac{2}{3}h + \tfrac{1}{3}k + \tfrac{1}{3}l) \tag{4}$$

The resultant structure factor F_{hkl}^{bulk} is obtained by summing over all layers which make up the truncated crystal:

$$F_{hkl}^{\text{bulk}} = \sum_{n=-\infty}^{0} F_{hkl}^{\text{layer}} \exp(in\psi_{hkl}) \exp(n\mu) = \frac{F_{hkl}^{\text{layer}}}{1-\exp(-i\psi_{hkl})\exp(-\mu)} \tag{5}$$

with μ an attenuation parameter, which can be neglected in practice.

The semi-infinite columns of bulk unit cells are covered by $(\sqrt{3}\times\sqrt{3})$R30° reconstructed surface unit cells, giving rise to fractional order reflections. For fractional order reflections there is no contribution from the bulk and the structure factor F_{hkl}^{sur} for the surface unit cell can be written as:

$$F_{hkl}^{\text{sur}} = \sum_j f_j^{hkl} \exp\left(\frac{-B_j\boldsymbol{Q}^2}{16\pi^2}\right) \times \exp[2\pi i(hx_j + ky_j + lz_j)] \tag{6}$$

where the summation extends over all atoms j with atomic coordinates x_j, y_j, and z_j in the surface unit cell. For the integer order rods the square of the total structure factor is computed as follows:

$$|F_{hkl}|^2 = (1-\Theta)|F_{hkl}^{\text{bulk}}|^2 + \Theta|3F_{hkl}^{\text{bulk}} + F_{hkl}^{\text{sur}}|^2 \tag{7}$$

Θ is the fraction of the surface that adopts the model surface structure. The factor three accounts for the difference in area between the bulk and surface unit cells, since there are three bulk unit cells within every surface unit cell. The atomic positions in the surface unit cell are fitted to the experimentally determined structure factors using a χ^2 minimization method.

3. Results

3.1. *Ag*(111)$(\sqrt{3}\times\sqrt{3})R30°$-*Sb*

First we investigate deposition of Sb on Ag(111) close to equilibrium. In Fig. 1 the intensity of the $(h\,k\,l) = (0\,1\,0.3)$ reflection is shown during deposition at a substrate temperature of 250°C. This reflection is very sensitive to stacking disorder, because atoms which grow at hcp sites interfere mainly constructively with the bulk, while atoms at the correct fcc sites interfere largely destructively. We can illustrate this with Eq. (4), where we find for this reflection for the correct fcc stacking a phase $\psi_{0\,1\,0.3} = 0.87\pi$. A layer of atoms at hcp sites is shifted with respect to the bulk over a translation vector $\boldsymbol{r}^{\text{stacking fault}} = \frac{1}{3}\boldsymbol{a}_1 + \frac{2}{3}\boldsymbol{a}_2 + \frac{1}{3}\boldsymbol{a}_3$. Then Eq. (4) becomes:

$$\psi_{hkl} = \boldsymbol{Q}\cdot\boldsymbol{r}^{\text{stacking fault}} = 2\pi(\tfrac{1}{3}h + \tfrac{2}{3}k + \tfrac{1}{3}l) \tag{8}$$

which gives $\psi_{0\,1\,0.3} = 1.53\pi$. The difference in intensity can be calculated by comparing the squared structure factor amplitudes for these situations:

$$\frac{|F_{0\,1\,0.3}^{\text{stacking fault}}|^2}{|F_{0\,1\,0.3}^{\text{bulk}}|^2} = 6 \tag{9}$$

After starting the deposition, first the intensity remains constant, indicating that the surface remains smooth. Therefore, the Sb atoms must dissolve in the top layer, as was also observed using scanning tunneling microscopy (STM) [14] and predicted by theoretical calculations [15].

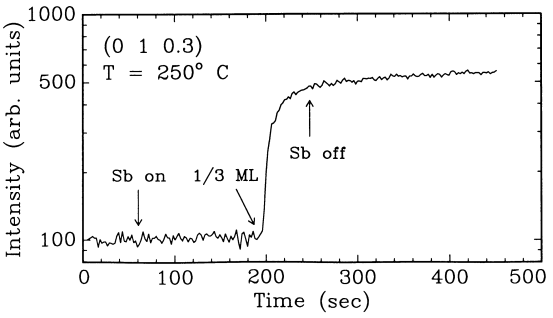

Fig. 1. The (0 1 0.3) reflection during Sb deposition at an Ag(111) substrate temperature of 250°C. After 1/3 ML the $(\sqrt{3}\times\sqrt{3})$R30° reconstruction is formed.

After 1/3 ML of Sb deposition, a sudden rise in intensity is seen, indicative of the abrupt formation of stacking faults. The intensity rise is almost the factor 6 calculated above, indicating that all top layer atoms, i.e. not only the Sb atoms, occupy hcp sites. This coincides with the formation of the $(\sqrt{3}\times\sqrt{3})$R30° reconstruction, as confirmed by measuring the $(\frac{1}{3}\,\frac{1}{3}\,0.2)$ reflection. From the measured peak FWHM we derived a correlation length L of 400 Å, where $L=2/\Delta Q_{\mathrm{FWHM}}$ [31].

The surface reconstruction was prepared twice, resulting in two data sets. For the first preparation 152 structure factors were measured, of which 106 were non-equivalent and for the second 104 reflections, of which 65 were non-equivalent. The uncertainty σ_{hkl} of the measured structure factor amplitudes was determined by quadratically summing the statistical and systematic error. The latter was estimated from symmetry equivalent reflections to be 10% for the first data set and 5% for the second. Total structure factor amplitudes measured along the (0 1), (0 2), and (1 1) CTRs are shown in Fig. 2, together with model calculations. These are plotted as a function of the diffraction index l, expressed in reciprocal lattice units (rlu). The negative l parts of the (0 1) and (0 2) rods were obtained by inverting the structure factor distribution along the positive $(0\,\bar{1})$ and $(0\,\bar{2})$ rods, respectively, through the origin of reciprocal space (Friedel's rule). The solid curves are calculated for our best-fit structural model. Dashed curves show calculations for an ideal, bulk-terminated Ag(111) surface.

A schematic of our model structure is shown in Fig. 3. Arrows indicate the allowed relaxation directions in our fit procedure. The total number of free fitting parameters was five, including a global scale factor, the surface fraction parameter Θ, and three atomic displacement parameters. The starting position of the Sb atoms was a hcp substitutional site, allowed to relax in the out-of-plane direction (parameter Δz_{Sb}). The two Ag atoms in the top layer were also situated at hcp positions and allowed to relax out-of-plane (parameter $\Delta z_{\mathrm{metal}}$). The three second layer Ag atoms below the Sb atom were allowed to relax laterally in the direction to (or from) the Sb atom (parameter Δx).

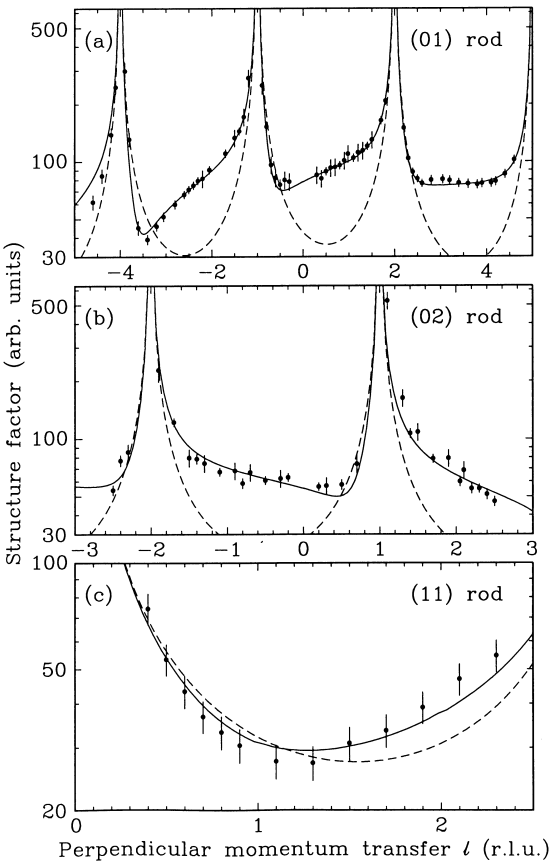

Fig. 2. Structure factor amplitudes $|F_{hkl}|$ along the (0 1), (0 2), and (1 1) crystal truncation rods measured on Ag(111)$(\sqrt{3}\times\sqrt{3})$R30°-Sb. Measured structure factors are indicated by filled circles. The dashed curves give calculations for the flat bulk-terminated Ag(111) surface and the solid curves represent calculations for our best-fit model.

In Fig. 4a the specular rod is shown, which is only sensitive to the out-of-plane positions of the atoms. Open circles represent measured data for clean Ag(111) and filled circles for the Sb-covered surface. For both surfaces, no significant surface roughness is found. Since the difference in scattering power between Sb ($Z=51$) and Ag ($Z=47$) is very small and only small relaxations occur, the fractional order reflections are very weak. In Fig. 4b the fractional order $(\frac{1}{3}\,\frac{1}{3})$ rod is shown.

The fit parameters and resulting nearest-neighbor distances for the atoms indicated in Fig. 3 are listed in Table 1. The best-fit atom coordinates are

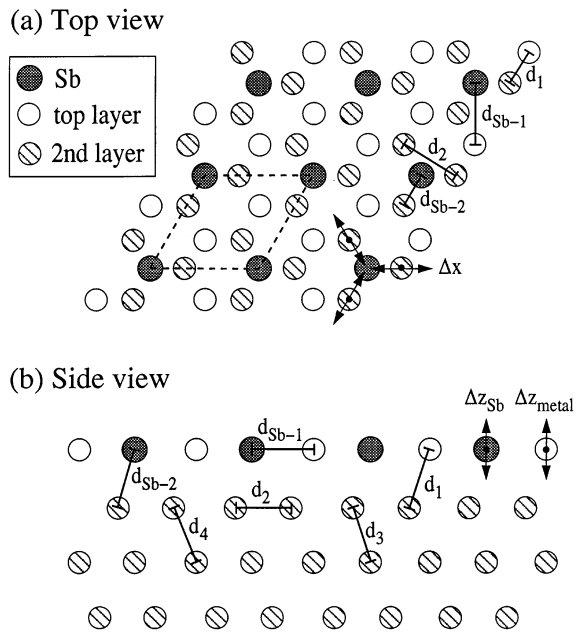

Fig. 3. Schematic projections of our structural starting model for both reconstructions in top view (a) and side view (b). The $(\sqrt{3}\times\sqrt{3})$R30° unit cell is indicated by the dashed lines. Arrows indicate the allowed relaxation directions in our fitting procedure. The indicated nearest-neighbor distances as derived from our best-fit model are given in Table 1.

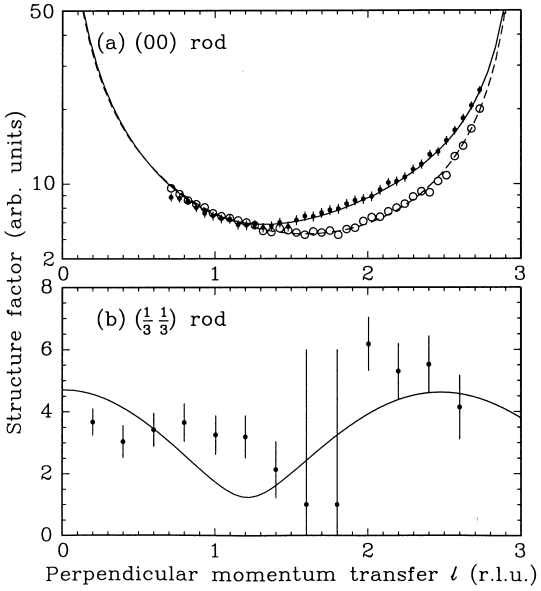

Fig. 4. (a) The specular rod for the clean (open circles) and Sb-covered (filled circles) Ag(111) surface. The dashed curve gives a calculation for bulk-terminated Ag(111) and the solid curve represents our model calculation. (b) Structure factor amplitudes $|F^{sur}_{hkl}|$ along the fractional order $(\frac{1}{3}\frac{1}{3})$ rod. Note that here the y-axis has a linear scale.

listed in Table 2. Our best-fit model has a reduced χ^2 of 1.3. All top layer atoms have relaxations out of the surface plane. The bulk distance between two (111) planes is 2.36 Å. Relative to this distance the Sb atom relaxes outwards by 0.17 Å and the two Ag atoms by 0.14 Å. The in-plane displacement of the second layer Ag atoms in the direction of the Sb atom is 0.06 Å. The reduced χ^2 did not improve significantly by allowing these three atoms to relax in the direction perpendicular to the surface plane.

Our integer order rods are rather insensitive to the small displacements in the surface plane. In fact, an almost equally good fit ($\chi^2=1.4$) is obtained when the in-plane relaxations are in the opposite direction. However, when we use in the fitting procedure only the in-plane part of the data set, χ^2 goes up from 2.7 (best fit) to 4.2. Without in-plane relaxations χ^2 becomes 6.4. Ag and Sb atoms have essentially identical "size", as judged

Table 1
Best-fit parameters and reduced χ^2 values for the structural models for Ag(111)$(\sqrt{3}\times\sqrt{3})$R30°-Sb and Cu(111) $(\sqrt{3}\times\sqrt{3})$R30°-Sb. The resulting nearest-neighbor atomic distances for the surface atoms (see Fig. 3) are given as well as the values for the nearest-neighbor distance in bulk Ag and Cu

Fit parameter	Ag(111) $(\sqrt{3}\times\sqrt{3})$ R30°-Sb	Cu(111) $(\sqrt{3}\times\sqrt{3})$ R30°-Sb
Θ surface fraction	0.75(3)	0.71(2)
Δz_{Sb} (Å) Sb out-of-plane	0.17(6)	0.49(2)
Δz_{metal} (Å) top Ag/Cu out-of-plane	0.14(3)	−0.11(2)
Δx (Å) second layer Ag/Cu in-plane	0.06(5)	0.012(6)
χ^2	1.3	1.3
Nearest-neighbor distances (Å)		
d_{Sb-1}	2.89(1)	2.63(1)
d_{Sb-2}	2.99(8)	2.97(3)
d_{bulk} (Ag/Cu)	2.89	2.56
d_1	3.02(3)	2.47(2)
d_2	2.78(8)	2.54(1)
d_3	2.85(2)	2.55(1)
d_4	2.91(1)	2.56(1)

Table 2
Structural parameters for the best-fit models of Ag(111)($\sqrt{3}\times\sqrt{3}$)R30°-Sb and Cu(111)($\sqrt{3}\times\sqrt{3}$)R30°-Sb (see Fig. 3). The atom positions in the surface unit cell are given by $\boldsymbol{r}=x\boldsymbol{a}_1+y\boldsymbol{a}_2+z\boldsymbol{a}_3$, with $\{\boldsymbol{a}_i\}$ the fundamental translation vectors as defined in Eq. (1). Fixed values are indicated by an asterisk (*). Deeper layers are fixed at bulk positions

		x	y	z		x	y	z
Top layer	Sb	0.000*	0.000*	0.690	Sb	0.000*	0.000*	0.745
	Ag	0.000*	1.000*	0.686	Cu	0.000*	1.000*	0.649
	Ag	1.000*	1.000*	0.686	Cu	1.000*	1.000*	0.649
Second layer	Ag	0.679	1.358	0.333*	Cu	0.669	1.339	0.333*
	Ag	0.642	0.321	0.333*	Cu	0.661	0.331	0.333*
	Ag	−0.321	0.321	0.333*	Cu	−0.331	0.331	0.333*

from their nearest-neighbor distances in bulk Ag (2.89 Å) and bulk Sb (2.90 Å). In Sb–Ag compounds the distance between Ag and Sb is about 2.97 Å. The nearest-neighbor distances in our model deviate from these values by less than 4%. Even in the surface case, which has more degrees of freedom, it appears that almost perfect substitution takes place.

3.2. *Cu*(111)($\sqrt{3}\times\sqrt{3}$)*R*30°-*Sb*

For Sb on Cu(111) we find similar results as for Ag(111). In Fig. 5 the intensity of the (0 1 0.9) reflection is shown during Sb deposition on Cu(111) at 450°C. Initially, the intensity increases slowly, after which it rises steeply and levels off to a constant value. The (0 1 0.9) reflection is even more sensitive to stacking faults than the (0 1 0.3) which was monitored for Ag(111) (Fig. 1).

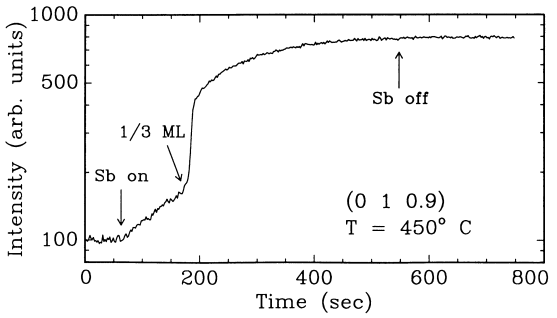

Fig. 5. The (0 1 0.9) reflection during Sb deposition on Cu(111) at 450°C. After 1/3 ML the ($\sqrt{3}\times\sqrt{3}$)R30° reconstruction is formed.

Because the scattering power difference between Sb ($Z=51$) and Cu ($Z=29$) is rather large, we find for Eq. (9) an intensity increase of factor 10 for a complete stacking fault layer with 1/3 ML of Sb. Without the stacking fault, this factor is 2 (because of the difference in Z, the Sb is observable in this case, unlike for Ag in Fig. 1). This explains why first the intensity rises by almost a factor 2 when the coverage comes close to 1/3 ML. Thus, analogous to the case of Ag(111), the Sb atoms dissolve in the top layer. Then the ($\sqrt{3}\times\sqrt{3}$)R30° reconstruction is formed with all the top layer atoms at stacking fault positions, resulting in an intensity rise of almost factor 10. During cool down to room temperature, the intensity remains the same. No significant surface roughness is found after deposition. By measuring the fractional order ($\frac{1}{3}\frac{1}{3}$ 0.2) reflection, we estimated the correlation length L to be 380 Å.

In total, 205 structure factors were measured, of which 83 were non-equivalent. The uncertainty for this data set was estimated to be 10%. In Fig. 6, the data for the integer order (0 1) rod, the specular rod, and the fractional order ($\frac{1}{3}\frac{1}{3}$) rod are shown together with our best-fit model calculations (solid curves). The dashed curves show calculations for bulk-terminated Cu(111).

The best-fit model parameters, atom coordinates, and resulting nearest-neighbor distances are listed in Tables 1 and 2. An important difference with the structure of the Ag($\sqrt{3}\times\sqrt{3}$)R30°-Sb reconstruction is a reversal of the perpendicular relaxation direction of the Cu atoms. We find that

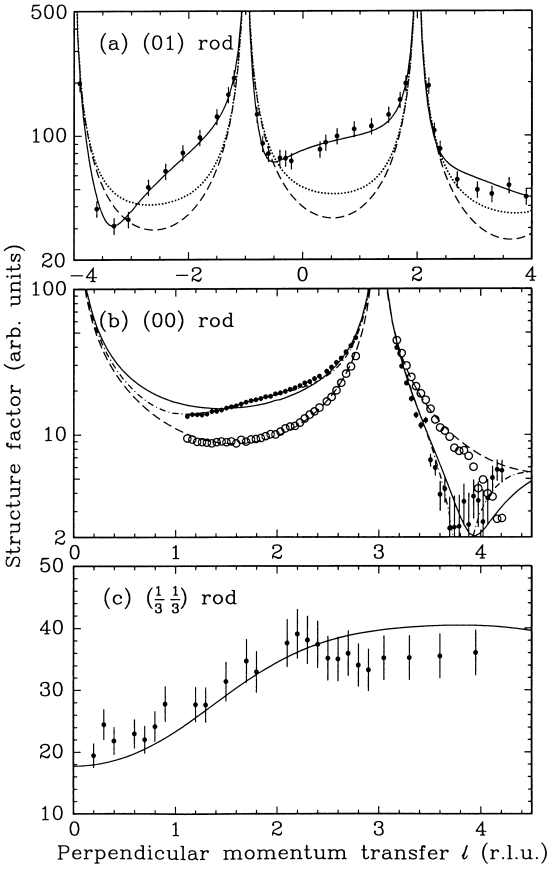

Fig. 6. Structure factor amplitudes along the (0 1), (0 0), and $(\frac{1}{3}\frac{1}{3})$ crystal truncation rods for Cu(111)$(\sqrt{3}\times\sqrt{3})$R30°-Sb. Measured structure factors are indicated by filled circles. The open circles in (b) are measurements of clean Cu(111). The dashed curves give the calculation for the bulk-terminated Cu(111) surface and the solid curves represent best-fit model calculations. In (a) the dotted curve represents a calculation for a structural model where the Sb atom is at a "normal" substitutional fcc site. For the specular rod in (b) the dashed–dotted curve represents a calculation for an extra Sb atom on top of the surface (see text).

the Sb atoms relax outwards by an amount 0.49 Å, but the Cu atoms relax inwards by 0.11 Å. This represents 5% of the bulk (111) interplanar distance of 2.09 Å. The in-plane relaxation of the second layer Cu atoms in the direction of the Sb atoms is estimated to be only 0.01 Å.

A model for which the Sb relaxes inwards and the two top layer Cu atoms outwards gives an equally good fit. However, the distance $d_{\mathrm{Sb-1}}$ then becomes 2.42 Å, and d_1 2.94 Å. Both these distances are clearly unphysical and can therefore be excluded. In Cu_2Sb the nearest-neighbor distances of Sb and Cu are 2.63 Å, 2.71 Å, and 2.84 Å, which come close to our best-fit results of 2.63 Å and 2.97 Å. The nearest-neighbor Cu–Cu distance d_1 is reduced by 4% compared to the bulk value.

The agreement between our model and the measured specular rod is good, but there are statistically significant deviations not explained by the model, particularly in the range $1<l<2$. Since the specular reflectivity probes the electron density distribution perpendicular to the surface, atoms which do not follow the lateral periodicity on the surface also contribute to the scattering. The deposition of Sb on the surface was stopped at an arbitrary position in time, but definitely past the place where the surface orders. Presumably there are Sb clusters at some parts on the surface. If we assume 0.06 ML of extra Sb atoms at arbitrary fixed positions on top of the surface, we obtain the dashed–dotted curve. This may not be a physically realistic model, but it shows that a small amount of extra Sb on top can make a large difference in the specular reflectivity.

4. Discussion

The sudden formation of the $(\sqrt{3}\times\sqrt{3})$R30° reconstruction as a function of the Sb coverage, as shown in Figs. 1 and 5, bears a striking resemblance to the phase transition in the exact solvable hard-hexagon model in statistical mechanics [32]. In this model hexagons can be positioned on three different sites, but may not overlap (hence the name of the model). In our case these hexagons can be associated with the Sb atoms which have three equivalent sites. In the hard-hexagon model there is a critical coverage above which the phase orders: $\rho_c=(5-\sqrt{5})/10=0.28$. Below this coverage, the three sites are randomly occupied, in agreement with STM [14]. A perfect $(\sqrt{3}\times\sqrt{3})$R30° reconstruction would have a coverage of 1/3 ML. The intensity rise depicted in Fig. 1 is estimated to be after deposition of 0.31(3) ML Sb.

The value of 0.28 is just within our error bar. In our best-fit models we find for the surface fraction parameter Θ values of 0.75 and 0.71, corresponding to an ordered Sb coverage of 0.25 and 0.23 ML, respectively. Part of the Sb atoms are not involved in the reconstruction. Even though these values are close to the value of 0.28, the difference from the ideal coverage of 1/3 ML may be fully explained by the possibility that not the entire surface is reconstructed. The qualitative agreement with the hard-hexagon model strongly suggests that the main driving force of the $(\sqrt{3}\times\sqrt{3})R30^\circ$ reconstruction is the repulsive interaction between Sb atoms.

For both reconstructions we find in essence a very similar surface atomic structure. The hcp site for the top layer atoms is energetically favored for both Ag and Cu. Comparing the fit parameters listed in Table 1, we see that differences occur only in the out-of-plane relaxations. This is a purely geometrical effect. Sb and Ag are similar in size, while Cu is significantly smaller. On the Cu substrate, the Sb atoms therefore need more space and the out-of-plane relaxation of the Sb atoms is much larger than on Ag(111). At the same time, the top layer Cu atoms are pushed towards the surface. This unusual embedded substitutional structure for an adsorbate–metal structure involving larger Z adatoms was already proposed years ago for Te ($Z=52$, about the same size as Sb) on Cu(111) [33]. For both reconstructions our models result in reasonable distances between the Sb and metal atoms. Because of the relaxation of the Cu atoms towards the surface, the distance between the Cu top and second layer atoms decreases with respect to the bulk nearest-neighbor distance. This is also the case for clean Cu(111), for which a top-layer spacing contraction of 0.7% relative to the layer spacing in the bulk was reported [34]. This corresponds to a nearest-neighbor distance d_1 of 2.54 Å.

To distinguish between three possible structural models, Noakes et al. [17] have compared coaxial impact collision ion scattering spectroscopy data taken on Ag(111)$(\sqrt{3}\times\sqrt{3})R30^\circ$-Sb to hitting probability simulations. Two models assume a simple Sb overlayer, where the Sb atoms can either occupy fcc or hcp sites. A third model involves the substitution of one top layer Ag atom per surface unit cell by an Sb atom. From their measurements they conclude that the correct model of the surface structure is that based on this substitutional adsorption site. From our observation of the growth as depicted in Fig. 1, we can conclude that the overlayer models can be ruled out, as also reported by STM measurements [14] and predicted by theoretical calculations [15]. We can also rule out the substitutional model by looking at the data of e.g. the (0 1) rod. The expected structure factor distribution for this substitutional model is indistinguishable from the calculation for the clean Ag(111) surface (dashed curve in Fig. 2a). This is because Ag has (almost) the same scattering power. Because Cu has a smaller Z, we can illustrate the substitutional model better for the Cu(111) $(\sqrt{3}\times\sqrt{3})R30^\circ$-Sb case. The dotted curve in Fig. 6a shows a calculation for this structure. The intensity contribution from the surface (in between the Bragg peaks) is slightly higher because of the additional scattering power from the Sb atoms in the surface layer. The extra interference effect we observe in our data because of the hcp stacking is absent. The ion scattering spectroscopy data of Noakes et al. [17] is more sensitive to the fact that the Sb atoms are embedded than to the stacking of the top layer. In that sense these data agree with our model.

In theoretical calculations [15] as well as in experiments of Cruguel et al. [18], another structural model was considered, namely one where the Sb is substituted in the second layer below the surface. On the same grounds as for the top layer substitutional site, we can confirm that this is not a correct model. The theoretical calculations [15] have shown that the substitutional site for Sb is considerably more favorable than an overlayer fcc site and than subsurface sites, but the stacking fault adsorption geometry we found was not considered. For the substitutional Sb an outward relaxation was predicted of about 0.25–0.35 Å, which is a rather large number. We have determined the outward Sb relaxation to be 0.17 Å (on the hcp site). In the calculations no outward relaxation of the Ag atoms was taken into account,

but here we have shown that these are also significant: 0.14 Å. The difference in height between the Sb and Ag atoms is thus small, which is consistent with STM measurements for the $(\sqrt{3}\times\sqrt{3})R30^\circ$ reconstruction as well as for the 1×1 phase for Sb coverages below 1/3 ML [13].

Very recently, our model has been corroborated. Medium energy ion scattering measurements performed on $Cu(111)(\sqrt{3}\times\sqrt{3})R30^\circ$-Sb are found to be consistent with the stacking fault position we propose [35].

Van der Vegt et al. [14] have studied the surfactant effect of Sb as a function of coverage up to 0.3 ML. They observed the nucleated island density to increase exponentially with Sb coverage. It is not known, however, what the influence of the $(\sqrt{3}\times\sqrt{3})R30^\circ$ reconstruction would be on this behavior. In an earlier study we have found that for sufficiently large Sb coverages, the top stacking fault layer described here is formed during Ag growth [11].

In conclusion, we have used the technique of surface X-ray diffraction to determine the structure of the reconstructed $Ag(111)(\sqrt{3}\times\sqrt{3})R30^\circ$-Sb and $Cu(111)(\sqrt{3}\times\sqrt{3})R30^\circ$-Sb surfaces. We find that the top layer atoms reside at stacking fault positions and each surface unit cell contains one substitutional Sb atom. We determined not only the registry of the top layer atoms, but also their out-of-plane relaxations. Furthermore, for the second layer we find small in-plane relaxations towards the Sb atoms.

Acknowledgements

We thank Patrick Knight, Steve Driver, and Wei Liu for their help during the measurements. René Koper is acknowledged for polishing the crystals. We thank Hubert Knops for introducing us to the hard-hexagon model. This work is part of the research program of the Foundation for Fundamental Research on Matter (FOM) and was made possible by financial support from the Netherlands Organization for Scientific Research (NWO). I.K.R. was supported by the US Department of Energy through Contract DEFG02-96ER45439.

References

[1] W.F. Egelhoff, I. Jacob, Phys. Rev. Lett. 62 (1989) 921.
[2] R. Kunkel, B. Poelsema, L.K. Verheij, G. Comsa, Phys. Rev. Lett. 65 (1990) 733.
[3] H.A. van der Vegt, H.M. van Pinxteren, M. Lohmeier, E. Vlieg, J.M.C. Thornton, Phys. Rev. Lett. 68 (1992) 3335.
[4] E. Bauer, H. Poppa, Thin Solid Films 12 (1972) 167.
[5] H.L. Gaigher, N.G. van der Berg, J.B. Malherbe, Thin Solid Films 137 (1986) 337.
[6] W.F. Egelhoff, D.A. Steigerwald, J. Vac. Sci. Technol. A7 (1989) 2167.
[7] B. Poelsema, R. Kunkel, N. Nagel, A.F. Becker, G. Rosenfeld, L.K. Verheij, G. Comsa, Appl. Phys. A 53 (1991) 369.
[8] S. Esch, M. Hohage, Th. Michely, G. Comsa, Phys. Rev. Lett. 72 (1994) 518.
[9] H.A. van der Vegt, W.J. Huisman, P.B. Howes, E. Vlieg, Surf. Sci. 330 (1995) 101.
[10] H.A. van der Vegt, J. Alvarez, X. Torrelles, S. Ferrer, E. Vlieg, Phys. Rev. B 52 (1995) 17443.
[11] S.A. de Vries, W.J. Huisman, P. Goedtkindt, M.J. Zwanenburg, S.L. Bennett, E. Vlieg, Phys. Rev. Lett. 81 (1998) 381.
[12] J.A. Meyer, H.A. van der Vegt, J. Vrijmoeth, E. Vlieg, R.J. Behm, Surf. Sci. 355 (1996) L375.
[13] J. Vrijmoeth, H.A. van der Vegt, J.A. Meyer, E. Vlieg, R.J. Behm, Phys. Rev. Lett. 72 (1994) 3843.
[14] H.A. van der Vegt, J. Vrijmoeth, R.J. Behm, E. Vlieg, Phys. Rev. B 57 (1998) 4127.
[15] S. Oppo, V. Fiorentini, M. Scheffler, Phys. Rev. Lett. 71 (1993) 2437.
[16] T.C.Q. Noakes, D.A. Hutt, C.F. McConville, Surf. Sci. 307–309 (1994) 101.
[17] T.C.Q. Noakes, D.A. Hutt, C.F. McConville, D.P. Woodruff, Surf. Sci. 372 (1997) 117.
[18] H. Cruguel, B. Lépine, S. Ababou, F. Solal, G. Jézéquel, Phys. Rev. B 55 (1997) R16061.
[19] H. Giordano, O. Alem, B. Aufray, Scr. Metall. 28 (1993) 257.
[20] H. Giordano, B. Aufray, Surf. Sci. 307–309 (1994) 816.
[21] P. Ma, A.J. Slavin, J. Vac. Sci. Technol. A11 (1993) 2003.
[22] I.K. Robinson, D.J. Tweet, Rep. Progr. Phys. 55 (1992) 599.
[23] S.R. Andrews, R.A. Cowley, J. Phys. C 18 (1985) 6427.
[24] I.K. Robinson, Phys. Rev. B 33 (1986) 3830.
[25] C. Norris, M.S. Finney, G.F. Clark, G. Baker, P.R. Moore, R. van Silfhout, Rev. Sci. Instrum. 63 (1992) 1083.
[26] E. Vlieg, A. van't Ent, A.P. de Jongh, H. Neerings, J.F. van der Veen, Nucl. Instrum. Meth. A262 (1987) 522.
[27] M. Lohmeier, E. Vlieg, J. Appl. Crystallogr. 26 (1993) 706.

[28] J.S.G. Taylor, C. Norris, E. Vlieg, M. Lohmeier, T.S. Turner, Rev. Sci. Instrum. 67 (1996) 2658.
[29] E. Vlieg, J. Appl. Crystallogr. 30 (1997) 532.
[30] C.H. Macgillavry, G.D. Rieck (Eds.), International Tables for X-ray Crystallography, vol. 3, Reidel, Dordrecht, 1983.
[31] E. Vlieg, J.F. van der Veen, S.J. Gurman, C. Norris, J.E. Macdonald, Surf. Sci. 210 (1989) 301.
[32] R.J. Baxter, Exactly Solved Models in Statistical Mechanics, Academic Press, London, 1982.
[33] F. Comin, P.H. Citrin, P. Eisenberger, J.E. Rowe, Phys. Rev. B 26 (1982) 7060.
[34] S.Å. Lindgren, L. Walldén, J. Rundgren, P. Westrin, Phys. Rev. B 29 (1984) 576.
[35] P. Bailey, personal communication.